Simple design of a wideband and wide-angle reflective linear polarization converter based on crescent-shaped metamaterial for Ku-band applications

Thi Quynh Hoa Nguyen [a,*], Thi Kim Thu Nguyen [a,b], Thi Quynh Mai Nguyen [a], Thanh Nghia Cao [a], Huu Lam Phan [a], Ngoc Minh Luong [a], Dac Tuyen Le [c], Xuan Khuyen Bui [d], Chi Lam Truong [e], Dinh Lam Vu [b]

[a] School of Engineering and Technology, Vinh University, 182 Le Duan, Vinh, Viet Nam
[b] Graduate University of Science and Technology, Vietnam Academy of Science and Technology, 18 Hoang Quoc Viet, Cau Giay, Hanoi, Viet Nam
[c] Department of Physics, Hanoi University of Mining and Geology, 18 Pho Vien, Hanoi, Viet Nam
[d] Institute of Materials Science, Vietnam Academy of Science and Technology, 18 Hoang Quoc Viet, Cau Giay, Hanoi, 100000, Viet Nam
[e] NTT Hi-Tech Institute, Nguyen Tat Thanh University, Ho Chi Minh city, Viet Nam

ARTICLE INFO

ABSTRACT

We report a wideband and wide-angle insensitive linear cross-polarization converter based on an anisotropic metamaterial. The converter structure consists of a periodic array of a top metallic crescent-shaped resonator and a bottom metallic ground plane separated by a dielectric layer of FR-4. Both simulation and experiment methods have performed to evaluate the proposed polarization converter performance. The results show a good agreement between the simulation and experimental results. The polarization converter efficiency above 90% is obtained for a wide bandwidth of 6 GHz covering the entire Ku-band (12–18 GHz) at normal incidence. Furthermore, the wideband polarization conversion properties are maintained with a large incident angle up to 45° for both transverse electric (TE) and transverse magnetic (TM) modes. Hence, the designed structure can be used for Ku-band applications.

1. Introduction

The manipulation of polarization state of the electromagnetic wave (EM) has attracted considerable interest due to its promising applications such as communications, imaging, and remote sensing [1]. Among polarization manipulation devices, polarization converters have been studied extensively for circularly polarized antennas [2,3] and radar cross section (RCS) reduction [4–6]. Recently, metamaterials are periodic or quasi-periodic planar arrays of sub-wavelength structures, have also been utilized in various applications such as perfect lens [7], invisible cloak [8], perfect absorber [9,10] and polarization converter [2,11]. Until now, polarization converters based on metamaterials have realized in the microwave [2,11], infrared [12,13] and visible [14–16] regimes because of their light weight and low profile.

Generally, the polarization converters can be designed to work in transmission and/or reflection modes. The polarization converters based on transmission mode demand multilayer structures, therefore, their fabrication is quite difficult, time-consuming, and costly. Meanwhile, the reflective polarization converters can be realized in a single-layer of metallic–dielectric–metallic configuration. In particular, the controllable design of reflective polarization converters based on single-layer that acts as linear-to-linear [17–26], linear-to-circular [27–30], circular-to-circular [31–34], and multifunctional [35–38] polarization conversion has been of great interest. Another desirable aspect of a reflective polarization converter design is that it can enlarge bandwidth to suitable for practical applications. The common method to extend the bandwidth of cross-polarization reflection is based on the anisotropic metamaterial that creates multiple resonances by electric and magnetic resonances [19,24,25]. The different dimensions of polarization converter structure formed by meandering line on resonator structure to various shapes such as split-ring with center disk [18], head arrow [19], V shape [20], L shape [21], U shape [22], H shape [25], and W shape [23,26] can create the different resonant peaks and the superposition of these multiple resonant peaks can expand the operation bandwidth. For example, Zhao et al. proposed a reflective linear polarization rotator based on split-ring with center disk resonator which achieves polarization conversion ratio (PCR) above 90% from 5.7 to 10.3 GHz with the relative bandwidth of 57.5% [18]. Xu. et al. reported an ultra-broadband reflective cross-polarization converter using the compact H-shaped metasurface, which achieves a relative bandwidth up to 94% in the frequency ranging from 7 to
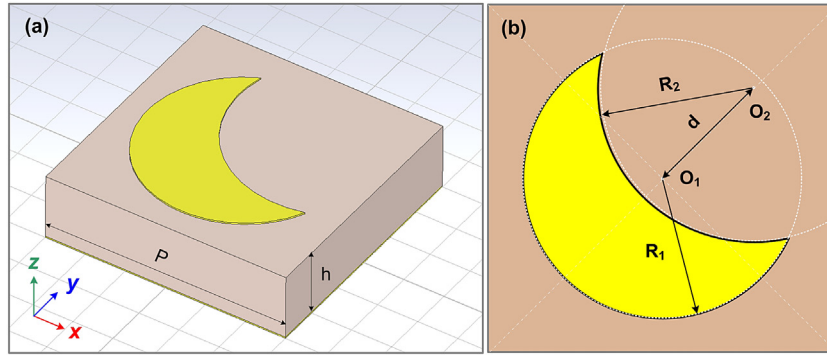

Fig. 1. Schematic of the proposed polarization converter: (a) 3D-view and (b) top-view of a unit cell.
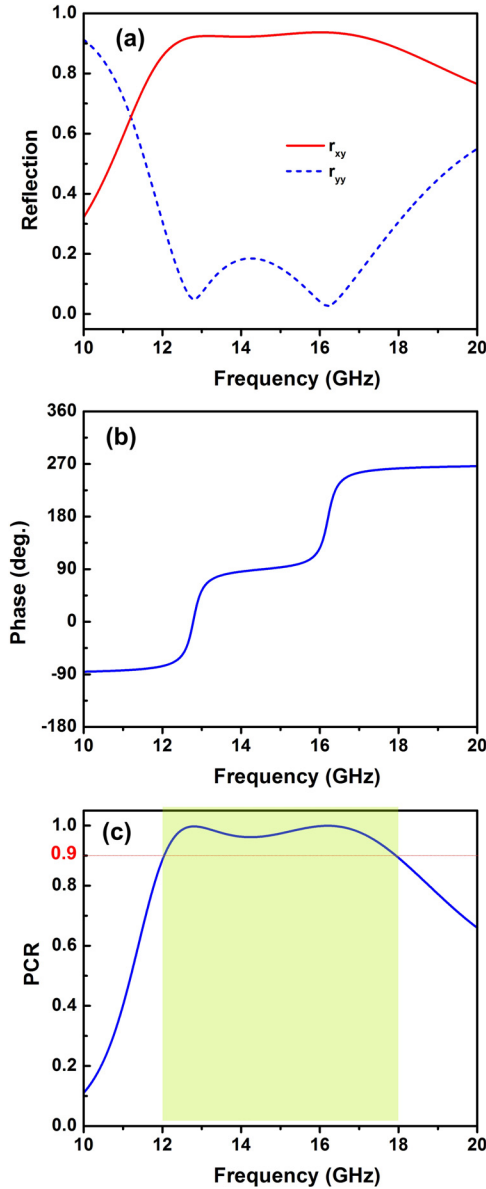

Fig. 2. (a) Magnitude and (b) phase difference of the reflection coefficients of co- and cross-polarizations, and (c) PCR of the proposed polarization converter at the normal incidence.
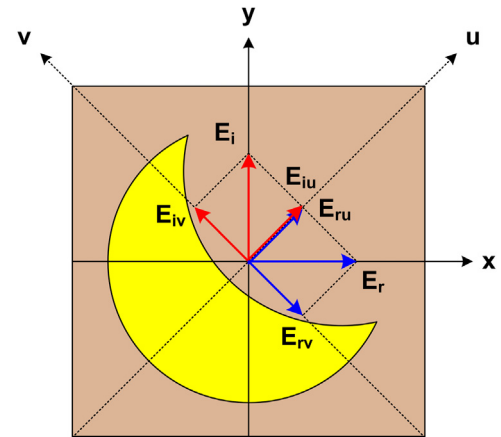

Fig. 3. Working principle of the proposed polarization converter.

19.5 GHz and the PCR higher than 90% [25]. Recently, Zhao et al. designed an ultra-wideband polarization rotator based on double W-shaped metasurface that can convert linearly polarized incident waves into its cross polarized reflective counterparts in the frequency range from 8.44 GHz to 24.96 GHz, and the relative bandwidth can be up to 99% [26]. Even though, these polarization converters revealed the wide bandwidth and high efficiency, however, the great limiting factor of meandering line based structures is the narrow angular tolerance due to the occurring of a dip in the operating frequency band with increasing of incident angle [18,20,25,26]. Therefore, the design of metamaterials for resolving this problem is well worth studying.

Herein, we propose a wideband and wide-angle insensitive reflective linear polarization converter based on single layer of anisotropic metamaterial for Ku-band applications. The proposed converter structure consists of a periodic array of a metallic crescent-shaped resonator and a bottom metallic ground plane separated by a dielectric substrate. The performance of the proposed structure is investigated by both simulation and experiment. The designed converter achieves a linear cross-polarization with the polarization converter ratio (PCR) greater than 90% in the whole Ku-band (12–18 GHz) with a relative bandwidth of 40% at normal incidence. Moreover, the high conversion efficiency is retained with a wide incident angle up to 45°. Thus, this designed structure can be applied for Ku-band applications.

2. Structure design and principle

In previously design, wideband linear polarization converters were used to design based on an anisotropic structure using meandering line such as L and V shapes. These polarization converter structures only efficiently convert the polarization of EM wave with narrow angle
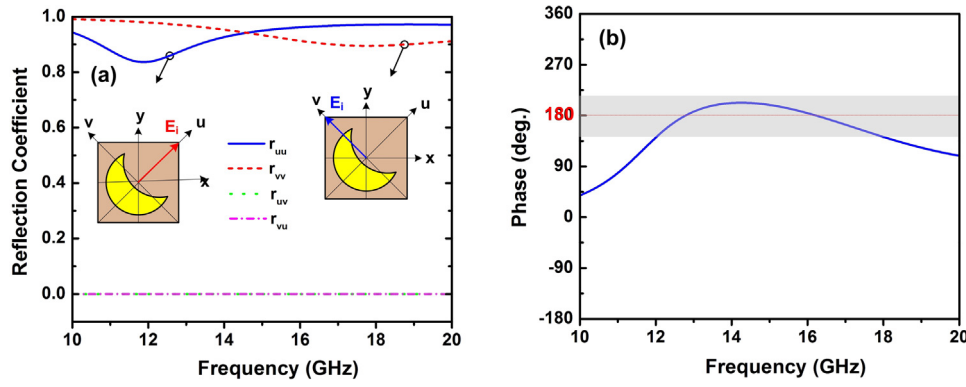
Fig. 4. (a) Magnitude and (b) phase difference of the reflection coefficients of *u*- and *v*-components for the proposed polarization converter at the normal incidence.
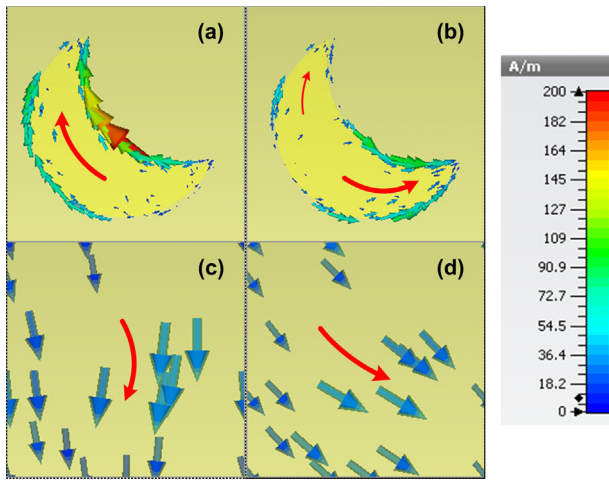

Fig. 5. Distributions of surface current on (a), (b) the top layer and (c), (d) the bottom layer of the proposed converter at the resonant frequencies of 12.8 GHz and 16.2 GHz, respectively.

tolerance due to the fact that the meandering line based structure can create absorption peak that leading to form the dip in their operating bandwidth with increasing of incident angle. Furthermore, the sharp corner features within these structures could also be difficult to fabricate with existing techniques such as photolithography. Therefore, in this study, we proposed the gradient structure based on crescent-shaped resonator to design a wideband linear polarization converter as presented in Fig. 1. Fig. 1 depicts a schematic of the unit cell of the proposed polarization converter. It is composed of a metallic crescent-sharped resonator and a metallic ground plane dielectric substrate spaced by a dielectric substrate, as shown in Fig. 1(a). The top and bottom layers are made of copper with a thickness of 0.035 mm and an electric conductivity of 5.96×10^7 S/m. The dielectric substrate is made by FR-4 with a thickness (h) of 1.6 mm and a relative dielectric constant of 4.3. The aim of the converter design is to work in the frequency range of 12–18 GHz. To reach this design purpose, we have optimized structural parameters by analyzing the effect of geometrical parameters of P in the range of 2.5–3.5 mm, R_1 in the range of 2.19–2.63 mm, R_2 in the range of 2.31–2.91 mm, and d in the range of 1.84–2.41 mm on the performance of the proposed polarization converter. The structural parameters are determined while considering both operating bandwidth and performance. Based on this analysis, the geometrical parameters of the unit cell are optimized as follows $P = 6$ mm, $R_1 = 2.41$ mm, $R_2 = 3.61$ mm, and $d = 2.12$ mm, as presented in Fig. 1(b). The centers of circles with radius R_1 and R_2 are O_1 (0 mm, 0 mm) and O_2 (1.5 mm and 1.5 mm).
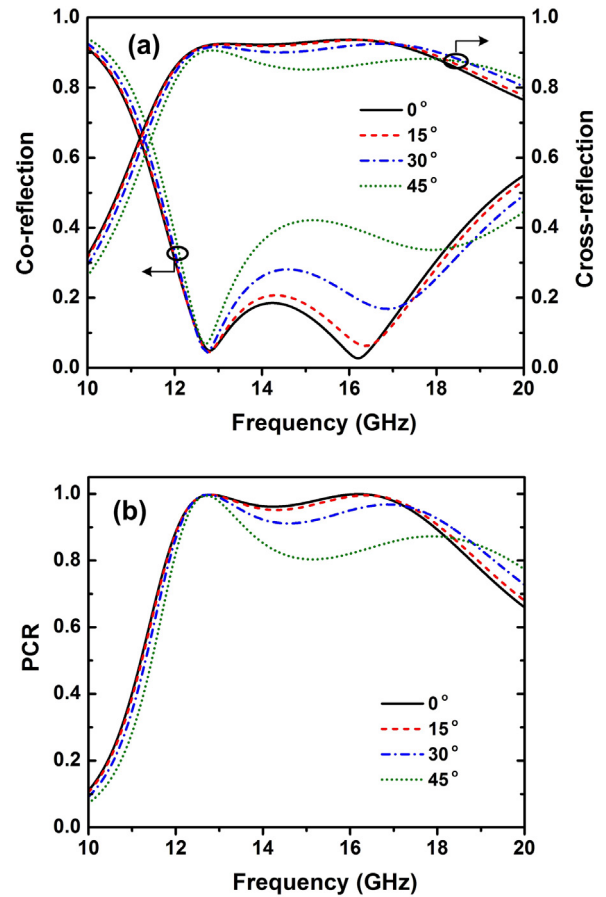

Fig. 6. (a) Magnitude of co- and cross-polarized reflection coefficients and (b) PCRs of the proposed polarization converter under TE mode for various incident angles.

To aid the design and analyze the performance of the polarization converter, the commercial computer simulation technology (CST) Microwave Studio software is used based on a frequency-domain solver [39]. In the simulation setup, the periodic boundary conditions are assigned to unit cell in the *x* and *y* directions, and the boundary condition is fixed to open in the *z*-direction. The simulation is performed in free space. Due to the symmetric of the unit cell along the diagonal direction, the co-and cross-polarized reflection coefficients for the *x*-axis are similar to those for *y*-axis. Therefore, we have just simulated for the *y*-polarized incident wave.
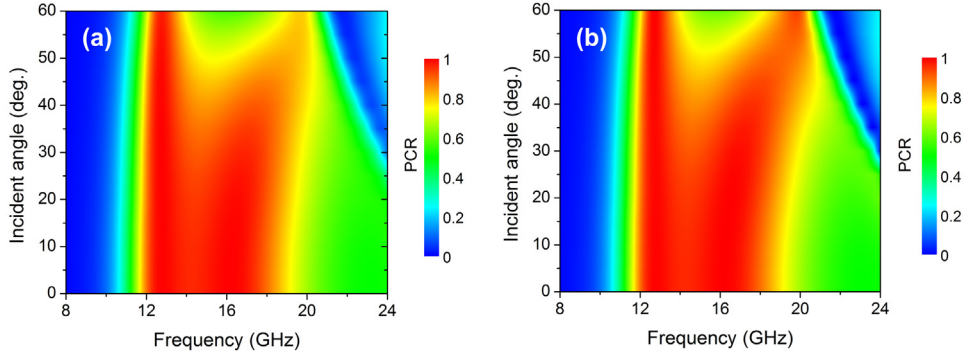
Fig. 7. PCR map as a function of the incident angle and of frequency for (a) TE and (b) TM modes.

3. Results and discussion

Fig. 2(a) shows the magnitude of co- and cross-reflection coefficients for the y-polarized incident wave under normal incidence. It can see that the magnitude of the co-reflection coefficient (r_{yy}) is below 0.19, while that of the cross-reflection coefficient (r_{xy}) is kept above 0.85 in a wide frequency range from 12 GHz to 18 GHz. Furthermore, the two distinct resonance peaks can be observed at 12.8 GHz and 16.2 GHz with the corresponding co- and cross-reflection coefficients of 0.05 and 0.92, and 0.03 and 0.94, respectively. The phase difference between the phase of the co- and the cross-polarization coefficient is depicted in Fig. 2(b). The phase difference ($\Delta\varphi$) is 90° or −90° in the whole band. It means that the perfect cross-polarization conversion can be revealed in the proposed converter for a wide frequency range.

To evaluate the polarization conversion performance of a linear polarization converter, the polarization converter ratio (PCR) is used that given by Eq. (1) [29,40].

$$PCR = \frac{\left|r_{xy}\right|^2}{\left|r_{xy}\right|^2 + \left|r_{yy}\right|^2} \tag{1}$$

where, $r_{xy} = \left|E_{rx}\right| / \left|E_{iy}\right|$ and $r_{yy} = \left|E_{ry}\right| / \left|E_{iy}\right|$ are cross-polarization and co-polarization reflection coefficients, respectively. E indicates the electric field while the subscripts x and y refer to the polarization directions and subscripts i and r represent the incident and reflected waves, respectively.

Fig. 2(c) presents the PCR curve of the proposed converter. At two resonance peaks of 12.8 GHz and 16.2 GHz, the PCR is approximately 100%. Moreover, the converter reveals the PCR above 90% in the frequency range from 12 GHz to 18 GHz with a relative bandwidth of 40%. This indicating that the designed converter can operate efficiently as a wideband linear polarization converter. The broadband response is due to the superposition of multiple resonance modes at 12.8 GHz and 16.2 GHz.

To demonstrate the working principle of the proposed polarization converter, we decompose the incident EM wave (E_i) into two orthogonal u- and v-directions as shown in Fig. 3. The u- and v-axes are inclined 45° and −45° to y-axis, respectively. Due to the asymmetric structure, the proposed converter obeys anisotropic characteristics with dispersive relative permittivity and permeability [24]. Therefore, the magnitudes and phases of reflection waves are different in u- and v-components. Given that r_{uu} and r_{vu} are magnitude of co- and cross-reflection coefficients for u-to-u and u-to-v polarization conversion, r_{vv} and r_{uv} are magnitude of co- and cross-reflection coefficients for u-to-u and v-to-u polarization conversion, and Φ_{uu} and Φ_{vv} are the phases for u-to-u and v-to-v polarization conversion, respectively. If $r_{uu} = r_{vv} \approx 1$, $r_{uv} = r_{vu} \approx 0$, and $\Delta\varphi = \left|\Phi_{uu} - \Phi_{vv}\right| \approx 180°$, the synthetic fields of E_{ru} and E_{rv} will be along the x-axis, as illustrated in Fig. 3. It implies that the incident polarized wave is rotated 90° and a cross-polarization conversion will be obtained.
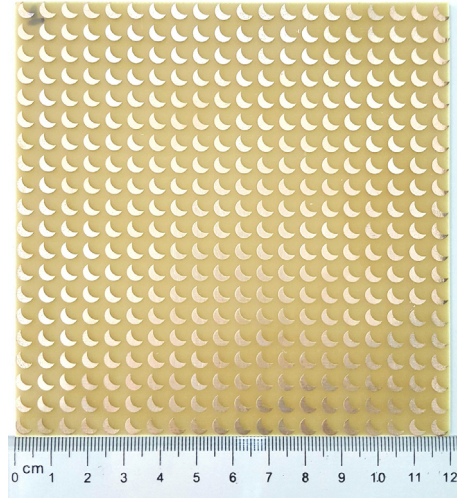

Fig. 8. The fabricated prototype of the converter consisting of 20 × 20 unit cells with a total dimension of 120 × 120 mm.

Fig. 4 represents the simulated magnitude of reflection coefficients and phase difference ($\Delta\varphi$) as a function of frequency when the EM incident wave is polarized along the u- and v-components. As shown in Fig. 4(a), the magnitude of the co-polarized reflection coefficient is close to 1 while magnitude of cross-polarized reflection coefficient is approximately 0 for almost frequencies. The phase difference between the u- and v-components is shown in Fig. 4(b). It can be seen that at two resonant frequencies of 12.8 GHz and 16.2 GHz, the phase difference is just exactly 180° and it is close to 180° in the frequency range from 12 GHz to 18 GHz. These obtained results prove that the designed converter achieves the wideband cross-polarization conversion performance.

To investigate the physical mechanism, the surface current distributions on the top and bottom metallic layer of the proposed converter are simulated at the resonant frequencies of 12.8 GHz and 16.2 GHz, as presented in Fig. 5. It can be seen from Figs. 5(a) and (c), at the resonant frequency of 12.8 GHz, the top and bottom surface current are anti-parallel to each other, resulting in the occurring of the circulating current in the dielectric layer. Therefore, this resonant frequency is considered as magnetic resonance. Meanwhile, at the higher resonant frequency of 16.2 GHz, the top surface current is divided into two regions where the currents on these regions are anti-parallel, as shown in Fig. 5(b). The bottom surface current is kept in the same direction (Fig. 5(d)). It means that the top surface current on one of regions is parallel and the top surface current of the other region is anti-parallel to the bottom surface currents, which generates both electric resonance and magnetic resonance, respectively. Thus, the higher resonant frequency is caused by both electric and magnetic resonances.
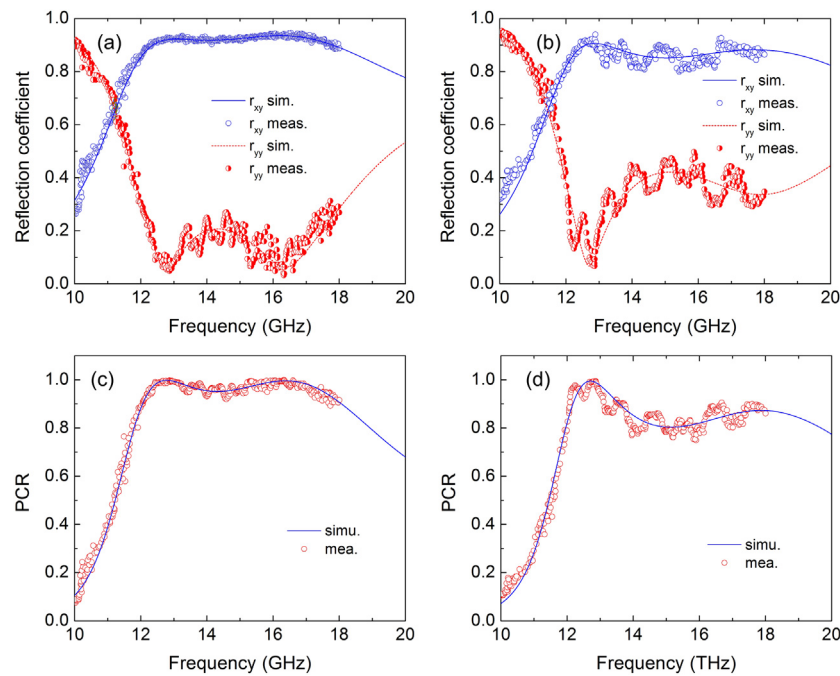
Fig. 9. (a), (b) Reflection coefficients and (c), (d) PCRs from simulation and experiment for normal incidence and oblique 45° incidence, respectively.

We also investigate the effect of incident angles on the performance of the proposed polarization converter. Figs. 6(a) and (b) show the magnitude of reflection coefficients and PCR curves of the proposed polarization converter with various incident angle under TE mode, respectively. It can be seen from Fig. 6(a), both the co- and cross-reflection coefficients have a small change with increasing the incident angle from 0° to 30° and a large change of these coefficients is observed with further increasing the incident up to 45°. Meanwhile, the bandwidth of the reflection coefficient seems unchanged with increasing the incident angle. Resulting, the PCR can keep higher than 90% in the operating frequency range from 12 GHz to 18 GHz when incident angle changes from 0° to 30°, as shown in Fig. 6(b). Even though, further increasing incident angle up to 45°, the PCR remains as high as 80%. Furthermore, the PCR map as a function of the incident angle and of frequency is simulated for both TE and TM modes, as represented in Fig. 7. The converter gives the PCR above 80% in the frequency range from 12 GHz to 18 GHz for both TE and TM modes. It means that the proposed polarization converter reveals a stable polarization conversion against changes the incident angle up to 45°.

Finally, to verify the design of the proposed polarization converter, we have fabricated the square sample with an oversize of 120 mm × 120 mm (20 × 20 unit cells) using the conventional printed circuit board process. The fabricated sample has the structural parameters the same as the simulated model. The image of the fabricated sample is shown in Fig. 8. The Rohde and Schwarz ZNB20 vector network analyzer together with two identical linearly polarized standard-gain horn antennas as transmitter and receiver is performed to characterize the reflection coefficients as a function of frequency. One horn antenna is used to emit *x*- or *y*-polarized waves, and the other horn antenna is used to receive *x*- and *y*-polarized waves. The separation angle between two antennas is set to be 10°, corresponding to the normal incidence measurement in the experimental. The co- and cross-polarized reflection coefficients are measured through the rotation of receive antenna by 0° and 90°, respectively. Figs. 9(a) and (b) show the measured magnitude of co- and cross-reflection coefficients at normal and 45° incidence, respectively, and the corresponding calculated PCRs are presented in Figs. 9(c) and (d). It indicates that the experimental results are in good agreement with the simulation results.

4. Conclusion

We have proposed a wideband and wide-angle insensitive linear polarization converter based on a single-layer of metal–dielectric–metal configuration. The proposed converter structure consists of a periodic array of a metallic crescent-shaped resonator and a bottom metallic ground plane separated by a dielectric spacer layer. The performance of the proposed converter has investigated by both simulation and experiment. The experimental and simulation result comparison was showed to be in good agreement. An investigation of the surface current distribution was simulated to explain the physical mechanism of the proposed polarization converter. The polarization converter exhibited a wideband linear cross-polarization in the entire X-band from 12–18 GHz with a relative bandwidth of 40% and a PCR above 90% at normal incidence. The high conversion efficiency can be maintained when the incident angle up to 45° for both TE and TM modes. Therefore, the designed structure can be suitable for Ku-band applications.

CRediT authorship contribution statement

Thi Quynh Hoa Nguyen: Conceptualization, Methodology, Writing, Supervision. **Thi Kim Thu Nguyen:** Data curation, Formal analysis. **Thi Quynh Mai Nguyen:** Data curation, Formal analysis. **Thanh Nghia Cao:** Software, Investigation. **Huu Lam Phan:** Data curation, Formal analysis. **Ngoc Minh Luong:** Software, Investigation. **Dac Tuyen Le:** Fabrication, Measurement. **Xuan Khuyen Bui:** Fabrication, Measurement. **Chi Lam Truong:** Software, Investigation. **Dinh Lam Vu:** Validation, Writing - reviewing.

Declaration of competing interest

The authors declare that they have no known competing financial interests or personal relationships that could have appeared to influence the work reported in this paper.

References

[1] N.K. Grady, J.E. Heyes, D.R. Chowdhury, Y. Zeng, M.T. Reiten, A.K. Azad, A.J. Taylor, D.A.R. Dalvit, H.-T. Chen, Terahertz metamaterials for linear polarization conversion and anomalous refraction, Science 340 (6138) (2013) 1304–1307.

[2] X. Ma, C. Huang, M. Pu, C. Hu, Q. Feng, X. Luo, Single-layer circular polarizer using metamaterial and its application in antenna, Microw. Opt. Technol. Lett. 54 (2012) 1770–1774.

[3] C. Yang, X. Zhu, P. Liu, W. Hong, H. Feng, Y. Shi, A circularly polarized horn antenna based on an FSS polarization converter, IEEE Antennas Wirel. Propag. Lett. 19 (2) (2020) 277–281, http://dx.doi.org/10.1109/LAWP.2019.2960013.

[4] Y. Liu, K. Li, Y. Jia, Y. Hao, S. Gong, Y.J. Guo, Wideband RCS reduction of a slot array antenna using polarization conversion metasurfaces, IEEE Trans. Antennas Propag. 64 (2016) 326–331.

[5] P. Su, Y. Zhao, S. Jia, W. Shi, H. Wang, An ultra-wideband and polarization-independent metasurface for RCS reduction, Sci. Rep. 6 (2016) 20387.

[6] Y. Jia, Y. Liu, Y.J. Guo, K. Li, S.-X. Gong, Broadband polarization rotation reflective surfaces and their applications to RCS reduction, IEEE Trans. Antennas Propag. 64 (1) (2016) 179–188.

[7] J.B. Pendry, Negative refraction makes a perfect lens, Phys. Rev. Lett. 85 (2000) 3966.

[8] D. Liang, J. Gu, J. Han, Y. Yang, S. Zhang, W. Zhang, Robust large dimension terahertz cloaking, Adv. Mater. 24 (2012) 916.

[9] N.I. Landy, S. Sajuyigbe, J.J. Mock, D.R. Smith, W.J. Padilla, Perfect metamaterial absorber, Phys. Rev. Lett. 100 (2008) 207402.

[10] T.S. Tuan, N.T.Q. Hoa, Numerical study of an efficient broadband metamaterial absorber in visible light region, IEEE Photonics J. 11 (3) (2019) 18648698.

[11] H.L. Zhu, S.W. Cheung, K.L. Chung, T.I. Yuk, Linear-to-circular polarization conversion using metasurface, IEEE T. Antenn. Propag. 61 (9) (2013) 4615–4623.

[12] H. Cheng, S. Chena, P. Yu, J. Li, B. Xie, Z. Li, J. Tian, Dynamically tunable broadband mid-infrared cross polarization converter based on graphene metamaterial, Appl. Phys. Lett. 103 (2013) 223102.

[13] Z. Zhang, J. Luo, M. Song, H. Yu, Large-area, Broadband and high-efficiency near-infrared linear polarization manipulating metasurface fabricated by orthogonal interference lithography, Appl. Phys. Lett. 107 (2015) 241904.

[14] Q.-T. Li, F. Dong, B. Wang, F. Gan, J. Chen, Z. Song, L. Xu, W. Chu, Y.-F. Xiao, Q. Gong, Y. Li, Polarization-independent and high-efficiency dielectric metasurfaces for visible light, Opt. Express 24 (15) (2016) 16309–16319.

[15] L. Yang, D. Wu, Y. Liu, C. Liu, Z. Xu, H. Li, Z. Yu, L. Yu, H. Ye, High-efficiency all-dielectric transmission metasurface for linearly polarized light in the visible region, Photonics Res. 6 (6) (2018) 517–524.

[16] Z.-H. Fang, H. Chen, D. An, C.-R. Luo, X.-P. Zhao, Manipulation of visible-light polarization with dendritic cell-cluster metasurfaces, Sci. Rep. 8 (2018) 9696.

[17] Y.Z. Cheng, W. Withayachumnankul, A. Upadhyay, D. Headland, Y. Nie, R.Z. Gong, M. Bhaskaran, S. Sriram, D. Abbott, Ultrabroadband reflective polarization convertor for terahertz waves, Appl. Phys. Lett. 105 (2014) 181111.

[18] J. Zhao, Y.i Cheng, A high efficiency and broadband reflective 90° linear polarization rotator based on anisotropic metamaterial, Appl. Phys. B 122 (2016) 255.

[19] H. Chen, J. Wang, H. Ma, S. Qu, Z. Xu, A. Zhang, M. Yan, Y. Li, Ultra-wideband polarization conversion metasurfaces based on multiple plasmon resonances, J. App. Phys. 115 (2014) 154504.

[20] X. Gao, X. Han, W.P. Cao, H.O. Li, H.F. Ma, T.J. Cui, Ultra-wideband and high-efficiency linear polarization converter based on double V-Shaped metasurface, IEEE T. Antenn. Propag. 63 (8) (2015) 3522–3530.

[21] Y. Jia, Y. Liu, W. Zhang, S. Gong, Ultra-wideband and high-efficiency polarization rotator based on metasurface, Appl. Phys. Lett. 109 (2016) 051901.

[22] Z.L. Mei, X.M. Ma, C. Lu, Y.D. Zhao, High-efficiency and wide-bandwidth linear polarization converter based on double U-shaped metasurface, AIP Adv. 7 (2017) 125323.

[23] Q. Zheng, C. Guo, P. Yuan, Y.H. Ren, J. Ding, Wideband and high-efficiency reflective polarization conversion metasurface based on anisotropic metamaterials, J. Electr. Mater. 47 (2018) 2658–2666.

[24] J. Xu, R. Li, S. Wang, T. Han, Ultra-broadband linear polarization converter based on anisotropic metasurface, Opt. Express 26 (20) (2018) 26235–26241.

[25] J. Xu, R. Li, J. Qin, S. Wang, T. Han, Ultra-broadband wide-angle linear polarization converter based on H-shaped metasurface, Opt. Express 26 (16) (2018) 20914–20919.

[26] Y. Zhao, B. Qi, T. Niu, Z. Mei, L. Qiao, Y. Zhao, Ultra-wideband and wide-angle polarization rotator based on double W-shaped metasurface, AIP Adv. 9 (2019) 085013.

[27] Y. Jiang, L. Wang, J. Wang, C.N. Akwuruoha, W. Cao, Ultra-wideband high-efficiency reflective linear-to-circular polarization converter based on metasurface at terahertz frequencies, Opt. Express 25 (22) (2017) 27616–27623.

[28] R. Swain, A. Chatterjee, S. Nanda, R.K. Mishra, A linear-to-circular polarization conversion metasurface based wideband aperture coupled antenna, J. Electr. Eng. Technol. 15 (2020) 1293–1299, http://dx.doi.org/10.1007/s42835-020-00402-z.

[29] M.I. Khan, Z. Khalid, F.A. Tahir, Linear and circular-polarization conversion in X-band using anisotropic metasurface, Sci. Rep. 9 (2019) 4552, http://dx.doi.org/10.1038/s41598-019-40793-2.

[30] Y.Z. Ran, L.H. Shi, J.B. Wang, S.B. Wang, G.M. Wang, J.G. Liang, Ultra-wideband linear-to-circular polarization converter with ellipse-shaped metasurfaces, Opt. Commun. 451 (2019) 124–128.

[31] Y. Cheng, J. Fan, H. Luo, F. Chen, N. Feng, X. Mao, R. Gong, Dual-band and high-efficiency circular polarization conversion via asymmetric transmission with anisotropic metamaterial in the terahertz region, Opt. Mater. Express 9 (2019) 1365–1376.

[32] X. Wu, Y. Meng, L. Wang, J. Tian, S. Dai, W. Wen, Anisotropic metasurface with near-unity circular polarization conversion, Appl. Phys. Lett. 108 (2016) 183502.

[33] M. Pan, Q. Li, Y. Hong, L. Cai, J. Lu, M. Qiu, Circular-polarization-sensitive absorption in refractory metamaterials composed of molybdenum zigzag arrays, Opt. Express 26 (2018) 17772–17780.

[34] X. Ma, C. Huang, M. Pu, C. Hu, Q. Feng, X. Luo, Multi-band circular polarizer using planar spiral metamaterial structure, Opt. Express 20 (14) (2012) 16050–16058.

[35] H. Jiang, W. Zhao, Y. Jiang, Frequency-tunable and functionality-switchable polarization device using silicon strip array integrated with a graphene sheet, Opt. Mater. Express 7 (2017) 4277–4285.

[36] P.C. Wu, W. Zhu, Z.X. Shen, P.H.J. Chong, W. Ser, D.P. Tsai, A.Q. Liu, Broadband wide-angle multifunctional polarization converter via liquid-metal-based metasurface, Adv. Opt. Mater. 5 (2017) 1600938.

[37] Y. Zhou, X. Cao, J. Gao, H. Yang, S. Li, Reconfigurable metasurface for multiple functions: Magnitude polarization and phase modulation, Opt. Express 26 (22) (2018) 29451–29459.

[38] J. Wang, R. Yang, R. Ma, J. Tian, W. Zhang, Reconfigurable multifunctional metasurface for broadband polarization conversion and perfect absorption, IEEE Access 8 (2020) 105815-105823.

[39] https://www.3ds.com/products-services/simulia/products/cst-studio-suite.

[40] J. Hao, Y. Yuan, L. Ran, T. Jiang, J.A. Kong, C.T. Chan, L. Zhou, Manipulating electromagnetic wave polarizations by anisotropic metamaterials, Phys. Rev. Lett. 99 (6) (2007) 063908.